

On discontinuous Galerkin discretizations of second-order derivatives

A. H. Hakim^{a,b}, G. W. Hammett^a, E. L. Shi^c

^a*Princeton Plasma Physics Laboratory, Princeton, NJ 08543-0451*

^b*Max-Planck/Princeton Center for Plasma Physics, Princeton University, Princeton, NJ*

^c*Department of Astrophysical Sciences, Princeton University, Princeton, NJ*

Abstract

Some properties of a Local discontinuous Galerkin (LDG) algorithm are demonstrated for the problem of evaluating a second derivative $g = f_{xx}$ for a given f . (This is a somewhat unusual problem, but it is useful for understanding the initial transient response of an algorithm for diffusion equations.) LDG uses an auxiliary variable to break this up into two first order equations and then applies techniques by analogy to DG algorithms for advection algorithms. This introduces an asymmetry into the solution that depends on the choice of upwind directions for these two first order equations. When using piecewise linear basis functions, this LDG solution g_h is shown not to converge in an L_2 norm because the slopes in each cell diverge. However, when LDG is used in a time-dependent diffusion problem, this error in the second derivative term is transient and rapidly decays away, so that the overall error is bounded. I.e., the LDG approximation $f_h(x, t)$ for a diffusion equation $\partial f / \partial t = f_{xx}$ converges to the proper solution (as has been shown before), even though the initial rate of change $\partial f_h / \partial t$ does not converge. We also show results from the Recovery discontinuous Galerkin (RDG) approach, which gives symmetric solutions that can have higher rates of convergence for a stencil that couples the same number of cells.

1. Introduction

Discontinuous Galerkin (DG) algorithms have been widely studied and fruitfully applied to a wide range of problems in recent years[1, 2, 3]. Here we focus on the problem of discretizing the second derivative of a known function. There are certain subtleties about the behavior of some algorithms for this problem, and understanding these can be helpful for understanding aspects of the algorithms for other problems, such as diffusion or elliptic problems.

Consider the problem of computing the discrete second derivative of a function, $f(x)$, given its projection $f_h(x)$ on a piecewise discontinuous polynomial space. Denoting $g(x) = f_{xx}$, the problem is to determine the best (in some L_2 sense) representation $g_h(x)$ on the same space. Discretization of such operators is required in a large number of problems involving diffusive processes. Our particular interest is to discretize certain forms of collision operators. For example, for small angle scattering in a plasma, the Lenard-Bernstein collision operator, $\mathcal{C}_{LB}[F(v)] = (\nu(v - u)F + \nu v_t^2 F_v)_v$, an approximation to the full Landau operator, is a combination of velocity space drag and diffusion, relaxing the distribution function to a Maxwellian. Even in the absence of an explicit diffusive process, a “hyper-collision” operator (involving terms such as f_{xxxx} or higher even-order derivatives) may be required to prevent momentum space filamentation and recurrence problems[4, 5, 6]. Subgrid models also require such operators to account for energy transfer to unresolved scales.

At present there are three broad techniques for including diffusive terms. The most popular approach is to introduce auxiliary variables to rewrite the second-order PDE as a system of first-order PDEs, and use the DG framework on the resulting larger system. This *local* DG[7] (LDG) approach leads naturally to estimates of solution derivatives at cell interfaces by particular choices of numerical fluxes for the introduced auxiliary variables. The second technique is to introduce special numerical fluxes, combined with “penalty” terms that penalize the solution for being discontinuous across interfaces[8]. These two techniques are not completely independent, and, in some ways, result from an attempt to apply ideas from finite-element methods to the DG discretization. See Ref [9] for a review of such methods.

The third technique is to reconstruct[10, 11] a continuous representation of the solution in the two cells sharing an interface and use that instead to compute the needed derivatives. This *recovery* DG (RDG) approach is closer in spirit to finite-volume methods in which solution gradients at cell interfaces, needed in Navier-Stokes equations, for example, are reconstructed using least-square fitting.

2. Testing discretizations of the second derivative operator

In this paper we look closely at the LDG and the RDG approaches for computing second derivatives both directly as well as for solving the diffusion and Poisson equations. To unify the presentation, assume piecewise linear expansion

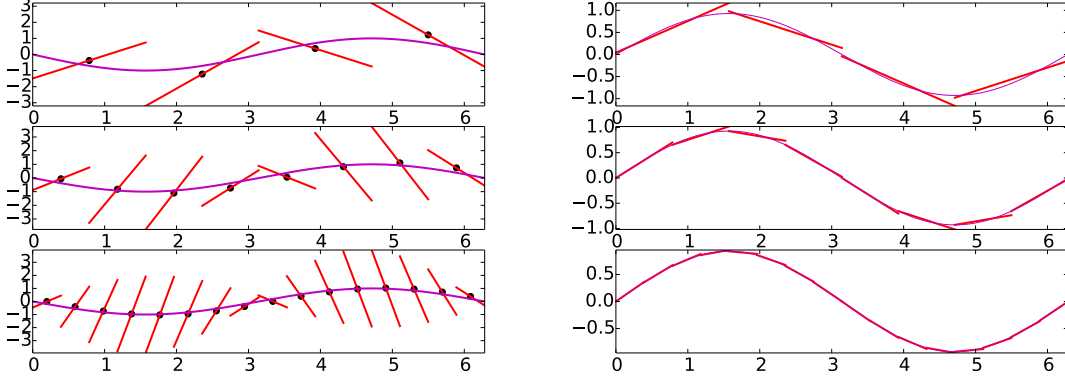


Figure 1: Second derivative of $\sin(x)$ (left panel) with 4 (top), 8 (middle) cells and 16 (bottom) cells using the asymmetric LDG scheme. Solution of diffusion equation $f_t = f_{xx}$ with $\sin(x)$ initial condition (right panel) with 4 (top), 8 (middle) cells and 16 (bottom) cells using the same asymmetric LDG stencil. The direct computation of second derivatives leads to a converging cell average (black dots), but a non-convergent and incorrect slope. In the time-dependent case, however, these errors decay very rapidly, leading to a convergent scheme. In each test $\sin(x)$ is *projected exactly* on linear basis functions. The right panels are plotted at $t = 0.075$, about the time of maximum error for the asymmetric LDG algorithm, as shown in Fig. 4.

$f_h(x, t) = f_{0,j} + f_{1,j}2(x - x_j)/(\Delta x)$ and $g_h(x, t) = g_{0,j} + g_{1,j}2(x - x_j)/(\Delta x)$ for $x \in [x_{j-1/2}, x_{j+1/2}]$, and where $x_j = (x_{j-1/2} + x_{j+1/2})/2$. For the LDG scheme rewrite $g = f_{xx}$ as a system of first order equations, $q = f_x$, $g = q_x$. Multiply by a test function and integrating over a cell j leads to a weak-form, which requires determining the values of $f_{j+1/2}$ and $q_{j+1/2}$ at cell boundaries. In the LDG approach, among several possible choices, one can pick, for example, $f_{j+1/2} = f_{j+1/2}^-$ and $q_{j+1/2} = q_{j+1/2}^+$, or $f_{j+1/2} = f_{j+1/2}^+$ and $q_{j+1/2} = q_{j+1/2}^-$ (these lead to the two forms of the asymmetric LDG we discuss below). With Legendre polynomials used as test and basis functions, for piecewise linear case, evaluating all terms explicitly, we can show that one form of the LDG scheme can be expressed as the stencil update

$$\begin{pmatrix} g_{0,j} \\ g_{1,j} \end{pmatrix} = \frac{1}{\Delta x^2} \begin{pmatrix} 4T^{-1} - 8I + 4T & 2T^{-1} + 2I - 4T \\ -12T^{-1} + 6I + 6T & -6T^{-1} - 24I - 6T \end{pmatrix} \begin{pmatrix} f_{0,j} \\ f_{1,j} \end{pmatrix}, \quad (1)$$

where the shift operators and its inverse are defined as $Tf_{k,j} = f_{k,j+1}$ and $T^{-1}f_{k,j} = f_{k,j-1}$, and $If_{k,j} = f_{k,j}$, where $f_{k,j}$ is the k -th moment of a modal expansion in Legendre polynomials in cell j . To derive these (and other) explicit forms of the update stencils, the auxiliary variable q is eliminated, and, on use of Legendre polynomial expansion, the stencil obtained. This stencil corresponds to the LDG method used for the diffusion operator part of Eq. 2.8 of Ref. [7], with \mathbb{C} in their Eq. 2.9 given by $c_{11} = c_{22} = 0$ and $c_{21} = -c_{12} = \sqrt{a}/2$ (and $a = 1$).

Note that the stencil is not symmetric in j , i.e., it is not symmetric with respect to the transformation $(x \rightarrow -x, f_{1,j} \rightarrow -f_{1,j}, g_{1,j} \rightarrow -g_{1,j})$, which corresponds to $(T \leftrightarrow T^{-1}, f_{1,j} \rightarrow -f_{1,j}, g_{1,j} \rightarrow -g_{1,j})$ in Eq. (1). This is a feature of the LDG scheme as one must make a choice of “upwind” directions to compute the numerical fluxes for the first-order system. In fact, one can derive another stencil by switching the order of the upwind directions, which corresponds to $c_{21} = -c_{12} = -\sqrt{a}/2$. Averaging the two asymmetric stencils, however, leads to a symmetric LDG stencil

$$\begin{pmatrix} g_{0,j} \\ g_{1,j} \end{pmatrix} = \frac{1}{\Delta x^2} \begin{pmatrix} 4T^{-1} - 8I + 4T & 3T^{-1} - 3T \\ -9T^{-1} + 9T & -6T^{-1} - 24I - 6T \end{pmatrix} \begin{pmatrix} f_{0,j} \\ f_{1,j} \end{pmatrix}. \quad (2)$$

Note that the asymmetric and symmetric stencils have the same terms on the diagonal, but different off-diagonal terms.

The recovery DG scheme starts from a weak-form. Multiply $g = f_{xx}$ by a test function $\varphi(x)$ and integrate over a cell to get

$$\int_{I_j} \varphi g dx = (\varphi f_x - \varphi_x f) \Big|_{x_{j-1/2}}^{x_{j+1/2}} + \int_{I_j} \varphi_{xx} f dx, \quad (3)$$

where integration by parts has been used twice. Note that as the function $f(x)$ is discontinuous across cell edges, a prescription is required to compute its value *and* its first derivative at cell edges.

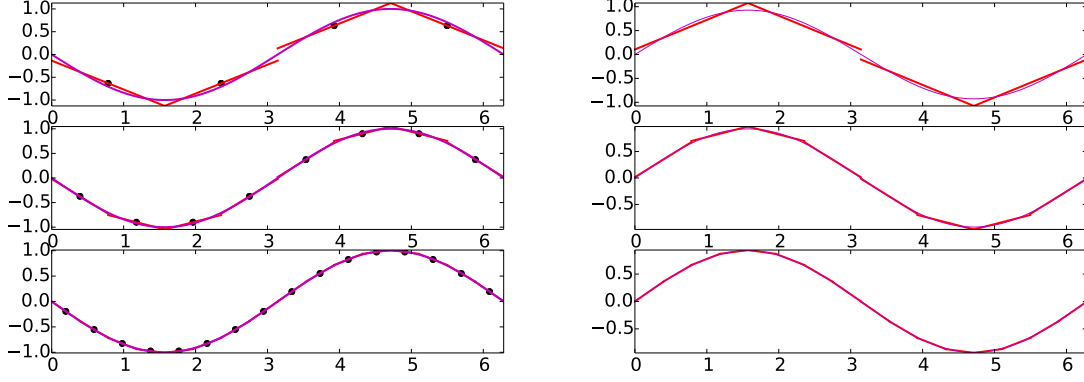


Figure 2: Same as Fig. (1), except using the RDG scheme. The cell average as well as the cell slope converge rapidly for computing the second derivatives as well as in the time-dependent problem. As seen from Fig. (4), the errors in the RDG are smaller than in either of the LDG schemes. The right panels are plotted at $t = 0.075$ as in Fig. 1.

The recovery discontinuous Galerkin (RDG) scheme proposed by van Leer and Nomura[11] replaces the function $f(x)$ at each edge by a *recovered* polynomial that is continuous across the cells shared by that edge. I.e., we write instead the weak form

$$\int_{I_j} \varphi g dx = (\varphi \hat{f}_x - \varphi_x \hat{f}) \Big|_{x_{j-1/2}}^{x_{j+1/2}} + \int_{i,j} \varphi_{xx} f dx, \quad (4)$$

where $\hat{f}(x)$ is the recovered polynomial, continuous across a cell edge. As the recovered polynomial is continuous, its derivative can be computed and used in the above weak-form. Consider an edge $x_{j-1/2}$. To recover a polynomial that is continuous in cells I_{j-1} and I_j that share this edge, we use L_2 minimization to give the conditions

$$\int_{I_{j-1}} (\hat{f} - f) \varphi_{j-1} dx = 0, \quad \int_{I_j} (\hat{f} - f) \varphi_j dx = 0 \quad (5)$$

for all test functions in the two cells, φ_{j-1} and φ_j . This ensures that \hat{f} , defined over $I_{j-1} \cup I_j$ is identical to $f(x)$ in the least-square sense, in the space spanned by the test functions φ_j . [For example, in the simplest DG case of piecewise constant basis functions, this procedure leads to an $\hat{f}(x)$ that is a linear function that matches the mean value in cells j and $j + 1$. For DG with p order basis functions, the full recovered $\hat{f}(x)$ would be a $2p + 1$ order polynomial, which we will use here. One could consider lower order recovery methods also, where $\hat{f}(x)$ was determined by projection onto a lower order subset of basis functions.] For the piecewise linear case, this procedure leads to the following stencil

$$\begin{pmatrix} g_{0,j} \\ g_{1,j} \end{pmatrix} = \frac{1}{4\Delta x^2} \begin{pmatrix} 9T^{-1} - 18I + 9T & 5T^{-1} + 5T \\ -15T^{-1} - 15T & -7T^{-1} - 46I - 7T \end{pmatrix} \begin{pmatrix} f_{0,j} \\ f_{1,j} \end{pmatrix}. \quad (6)$$

Note that the stencil is symmetric, which results from the fact that the recovery procedure does not distinguish the solutions in cells $j - 1$ and $j + 1$, as does the LDG scheme.

One way to think about the motivation for the RDG procedure is to consider that the general DG algorithm tells us how certain moments of the solution in each cell evolve in time, but there is flexibility in how to use that information to reconstruct a representation for $f_h(x)$. The standard DG approach uses only moment information in a single cell to construct a representation for $f_h(x)$ within that cell, which may be discontinuous with the representation in the neighboring cell. The RDG algorithm uses information from neighboring cells to reconstruct a locally continuous representation for $\hat{f}(x)$ to calculate the flux from the diffusive term, which avoids the problem that the flux would be infinite if the solution was discontinuous. In this regard, RDG is similar in philosophy to the reconstruction approach described in Ref. [12]. For the flux from the advection operator, one can still use the standard DG approach based on $f_h(x)$ from the upwind side of a cell face, thus preserving the property that advection should propagate information only in the downwind direction.

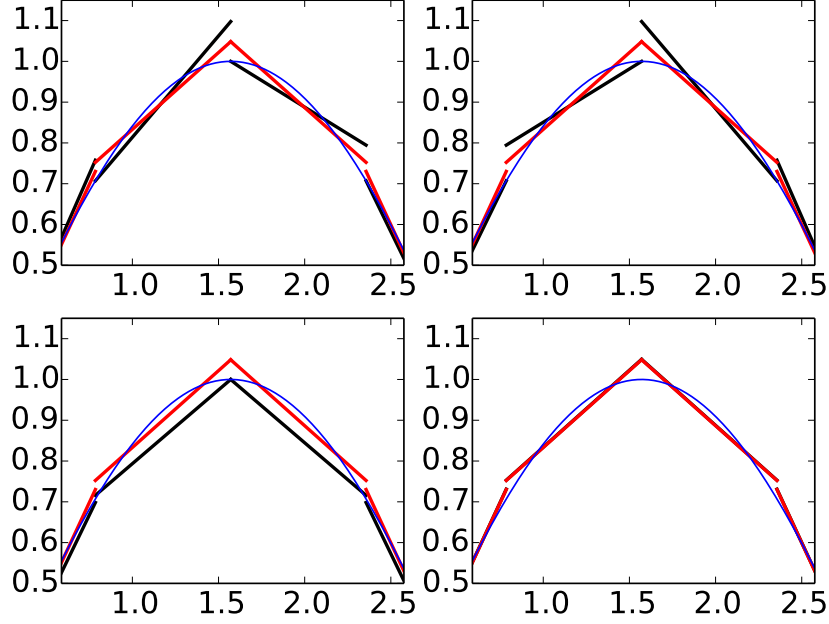


Figure 3: Solution to the Poisson equation $f_{xx} = -\sin(x)$ with piecewise linear basis functions on a grid of 8 cells, using the two asymmetric versions of LDG schemes (top row), symmetric LDG scheme (lower left) and RDG scheme (lower right). Only the solution around the maxima are shown. Black lines are numerical solutions and red lines are the projection of the exact solution $\sin(x)$ (shown as blue lines) onto piecewise linear basis functions. The LDG schemes show larger errors in the slopes than the RDG scheme (which matches the exact solutions very accurately). However, the LDG computed slopes converge to the correct result as the grid is refined.

Tests of the asymmetric LDG scheme and the RDG are shown in Figs. (1) and (2). These figures show that the LDG scheme, even though convergent for the solution of a diffusion equation, mispredicts the slope of f_{xx} .

This surprising behavior is confirmed by a Taylor series analysis. To do this, consider three cells, labeled $j \in \{-1, 0, 1\}$, centered around $x = 0$. For some function $f(x)$, consider the Taylor expansion

$$f_N(x) = \sum_{n=0}^N \frac{x^n}{n!} f^{(n)}(0), \quad (7)$$

where $f^{(n)}(0)$ is the n -th derivative evaluated at $x = 0$. Project $f_N(x)$ on the DG basis functions (Legendre polynomials, $P_k(\eta_j(x))$, with $\eta_j(x) = 2(x - x_j)/\Delta x$, where x_j is the cell center coordinate) in each cell j . Denote these projections by $F_{j,k}$. Use these projections in the stencil, for example, replacing Tf_k by $F_{+1,k}$, $T^{-1}f_k$ by $F_{-1,k}$ and If_k by $F_{0,k}$, to compute the expansion for the operator f_{xx} . Finally, projecting the resulting expansion back onto a Taylor basis in cell $j = 0$, yields the final Taylor expansion of $g_h(x)$.

For the asymmetric LDG stencil, Eq. (1), to leading order, the slope of $g_h(x)$ is $-6f_{xx}/\Delta x$. Note that the slope should be f_{xxx} , indicating that not only is the slope incorrect, but blows up as the mesh is refined. This behavior is confirmed quantitatively in Fig. (1). [Certain types of Taylor series analysis can give rise to misleading results because of supra-convergence phenomena, as discussed in Refs. [13, 14]. The result from the way we use Taylor series here is confirmed by a von Neumann-like analysis in the next section.] For the symmetric LDG scheme, Eq. (2), a Taylor series analysis shows that to leading order the slope is $3f_{xxx}/5$, i.e. although of the correct derivative order, with the wrong coefficient (which should be unity). On the other hand, for the RDG stencil, Eq. (6), to leading order the slope is f_{xxx} , as it should be. Also, a convergence study shows that a piecewise linear RDG scheme converges faster (fourth order accuracy) than the LDG schemes, which are second-order.

This incorrect behavior of the higher moments (higher than cell average) of g_h with LDG schemes also occurs with higher order basis functions. For example, one possible asymmetric LDG stencil with piecewise quadratic Legendre

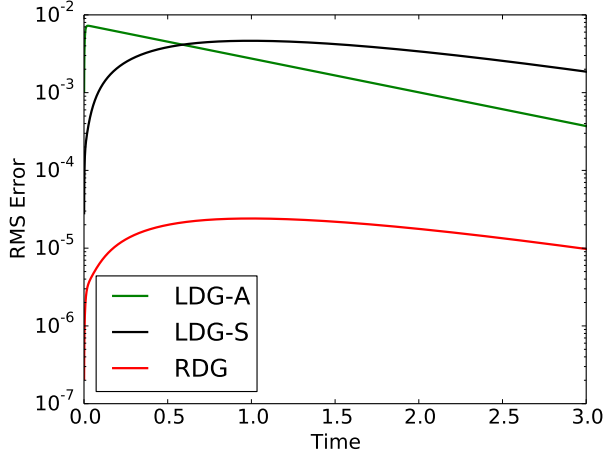


Figure 4: Time history of L_2 norm of the error in solution of the diffusion equation $f_t = f_{xx}$ on 16 cell mesh with the asymmetric LDG scheme (green), the symmetric LDG scheme (black) and the RDG scheme (red). The RDG scheme has the smallest error. Convergence tests show that the LDG schemes converge as Δx^2 , while RDG converges as Δx^4 .

polynomial basis functions is

$$\begin{pmatrix} g_{0,j} \\ g_{1,j} \\ g_{2,j} \end{pmatrix} = \frac{1}{\Delta x^2} \begin{pmatrix} 9T^{-1} - 18I + 9T & 7T^{-1} + 2I - 9T & 3T^{-1} - 12I + 9T \\ -27T^{-1} + 6I + 21T & -21T^{-1} - 54I - 21T & -9T^{-1} + 24I + 21T \\ 45T^{-1} - 60I + 15T & 35T^{-1} + 40I - 15T & 15T^{-1} - 90I + 15T \end{pmatrix} \begin{pmatrix} f_{0,j} \\ f_{1,j} \\ f_{2,j} \end{pmatrix}. \quad (8)$$

A Taylor series analysis of this stencil shows that, to leading order, the slope goes as $8f_{xxx}/5$ and the second moment goes as $-6f_{xxx}/\Delta x$. This shows that not only is the slope mispredicted, but the highest moment (which should be f_{xxxx}) blows up as $\Delta x \rightarrow 0$. In general, for higher order asymmetric LDG schemes, all moments are incorrect, with the highest moment blowing up as $1/\Delta x$. For the piecewise linear scheme, because the slope goes as $1/\Delta x$, the L_2 norm of the error will not converge to zero as the grid is refined. However, for higher order polynomial schemes, even though the errors at the cell boundary are $O(1)$, since the highest moment p goes only as $1/\Delta x$ (and not as $1/\Delta x^p$), the L_2 error in the approximation of g_h still converges to zero as the grid is refined.

3. Exact time dependence from a von Neumann-like analysis

The above results can also be demonstrated by calculating the full time dependence of the LDG solution for a diffusion equation, which can be done using a von Neumann-like analysis (with a Fourier expansion for the variations between cells, and an eigenmode analysis for the variations within a cell), as given in Ref. [14]. (We will follow their notation in this section. They solve a diffusion equation of the form $u_t = u_{xx}$, so their u is equivalent to our f .) They show how to work out the exact solution to the discretized LDG equations for $u_{j\pm 1/4}(t)$ (u evaluated at two equally-spaced points in the j 'th cell corresponding to LDG with piecewise linear basis functions). The initial condition is $u(x, t=0) = \sin(kx)$ (and $k=1$). Using a Fourier representation for the variation between cells ($u_{j+3/4} = u_{j-1/4} \exp(ik\Delta x)$, etc.), the solutions for $k\Delta x \ll 1$ are

$$u_{j-1/4}(t) = \sin(x_{j-1/4}) \left[e^{-t} + \frac{(\Delta x)^2}{24} (e^{-|\lambda_1|t} - e^{-t}) \right] + \mathcal{O}((\Delta x)^3) \quad (9)$$

(this extends to higher order the result in their unnumbered equation after Eq. 3.22), and

$$u_{j+1/4}(t) = \sin(x_{j+1/4}) \left[e^{-t} - \frac{(\Delta x)^2}{24} (e^{-|\lambda_1|t} - e^{-t}) \right] + \mathcal{O}((\Delta x)^3). \quad (10)$$

Here, λ_1 is the first of the two eigenvalues given in their Eq. 3.18, and is $\lambda_1 \approx -36/(\Delta x)^2$ for $k\Delta x \ll 1$. The exact solution to the analytic diffusion equation is $u = \sin(x)e^{-t}$, so one sees from the above two equations that the errors in u

from LDG are bounded for all time and converges like $(\Delta x)^2$. However, if we ask what the rate of change of the solution is, we get

$$\frac{du_{j\pm 1/4}}{dt} = \sin(x_{j\pm 1/4}) \left[-e^{-t} \pm \frac{3}{2} e^{-|\lambda_1|t} \right] + \mathcal{O}((\Delta x)). \quad (11)$$

Since the exact analytical solution is $\partial u(x, t)/\partial t = u_{xx} = -\sin(x)e^{-t}$, we see that there is an order unity error in the time-derivative of the solution at early times, but it quickly dies away in time. Note that the time-derivative of the cell average, $(d/dt)(u_{j-1/4} + u_{j+1/4})/2$, converges to the right answer, while the time-derivative of the slope $(d/dt)(u_{j+1/4} - u_{j-1/4})/(\Delta x/2) = -6/(\Delta x)$ is the same as we found in the Taylor series analysis around Eq. 7 above. This confirms that there are order unity errors in the discretization of the second derivative operator, but it also shows that these errors rapidly decay away in time when used in a diffusion equation, so that LDG converges to the right answer for diffusion problems.

[Ref. [14] evaluates the initial condition $\sin(x)$ at uniformly spaced grid points, though they point out that the more accurate thing to do is an L_2 projection of the initial condition onto the DG basis functions. We have repeated the von Neumann-like analysis with the more accurate L_2 projection, as is used elsewhere in this paper, and find that it changes some of the higher order terms, but not the term involving $\exp(-|\lambda_1|t)$ to the order kept here.]

As an aside, we point out that the two eigenvalues given by Eq. 3.18 of Ref. [14] are both physically meaningful (in contrast to some researchers who have called one eigenvalue/eigenvector as the “good” or physical mode, and the others as “bad” or unphysical modes). Because a Fourier representation $\exp(ikx_j)$ is used for the between-cell variation, $k\Delta x \in [0, \pi]$ covers the full range of possibilities. However, because $\exp(ikx_j)$ is periodic in k when evaluated at a set of uniformly spaced cell centers $x_j = j\Delta x$, one can consider k and $k' = k + 2\pi m/(\Delta x)$ (for integer m) as being equivalent. The second eigenvalue given by their Eq. 3.18 (which at long wavelengths $k\Delta x \ll 1$ is $\lambda_2 \approx -k^2$), corresponds to the usual eigenvalue for the d^2/dx^2 operator. The first eigenvalue is the discretized approximation to the d^2/dx^2 operator for an effective wave number $k_{\text{eff}} = k - 2\pi/\Delta x$, or using a reality condition to consider only positive k , can be taken to be an effective wave number of $k_{\text{eff}} = 2\pi/\Delta x - k$. This explains why λ_1 scales as $1/(\Delta x)^2 \sim k_{\text{eff}}^2$ for small $k\Delta x$. In general, a DG algorithm with N 'th order polynomial basis functions will lead to an amplification matrix $G(k, \Delta x)$ (such as in their Eq. 3.7) of size $(N+1) \times (N+1)$. This leads to $N+1$ eigenvalues for a given value of k that specifies the $\exp(ikj\Delta x)$ variation between cells, where $0 \leq k\Delta x \leq \pi$. These $N+1$ eigenvalues correspond to different modes with effective wavenumbers up to $k\Delta x = (N+1)\pi$, corresponding to the sub-cell variations that can be represented with higher order DG methods. (This is illustrated by plots of DG eigenvalues vs. $k\Delta x$ over the range $[0, (N+1)\pi]$, as shown in Figs. 1 and 3 of Ref. [11], and could be further illustrated by plots of the eigenfunctions.)

For the piecewise linear case studied here, even with an accurate L_2 projection of the initial condition $\sin(x)$ onto the DG basis functions, there is still a fraction $\propto (\Delta x)^2$ of the initial condition put in the high- k eigenmode of the LDG operator, which damps at the very fast rate $\lambda_1 \propto 1/(\Delta x)^2$, thus creating the order unity errors in $\partial u/\partial t = u_{xx}$ at early times. The RDG algorithm also has two eigenmodes per k , but the projection of the initial condition onto the RDG high- k eigenmode gives a much smaller value, so it converges when calculating a second derivative $g = f_{xx}$.

While the analysis in this section confirms that the error in the second derivative operator rapidly damps out in time for diffusion problems, one might wonder what the effect of this error is on problems where a second derivative term does not correspond to a dissipative effect, such as in the Schrödinger equation or in dispersive wave equations. Consider for example the normalized Schrödinger equation $i\partial u/\partial t = -u_{xx}$ with the initial condition $u(x, t=0) = \sin(x)$. The solution is as given in Eqs. 9-10, but with $t \rightarrow it$. Thus the solution for $-u_{xx}$ is

$$i\frac{du_{j\pm 1/4}}{dt} = \sin(x_{j\pm 1/4}) \left[e^{-it} \mp \frac{3}{2} e^{-|\lambda_1|t} \right] + \mathcal{O}((\Delta x)), \quad (12)$$

which has an order unity error at any time compared to the exact solution $i\partial u/\partial t = \sin(x)\exp(-it)$. Interestingly, however, an observable like the energy $E = -\langle u^* u_{xx} \rangle$ still properly converges (here $*$ denotes a complex conjugate), as can be seen by noting that $E \propto u_{j-1/4}^* i du_{j-1/4}/dt + u_{j+1/4}^* i du_{j+1/4}/dt$, so the errors from terms involving $\exp(-i|\lambda_1|t)$ cancel to lowest order. One might consider other ways to project initial conditions onto the discrete basis functions, such as by minimizing the error in a Sobolev norm instead of an L_2 norm. We leave further investigation of these issues for the Schrödinger equation or dispersive waves to future work.

4. Discussion and Conclusions

One may wonder why these errors in the discretized second derivative operator have not been noticed in the literature before. The main answer lies in the fact that the net effect of these errors is small when the same stencils are used in the solution of parabolic diffusion or elliptic Poisson equations (which is the steady-state solution of a diffusion equation). See

Figs. (1) and (2). That is, the errors in the slopes are modified in the time-dependent case, and damp out very quickly in time (or on operator inversion in an elliptic problem), so the solutions converge for those problems. This is because the component of $f_h(x)$ with a large error in the eigenvalue for the discretized operator $\partial^2/\partial x^2$ is at small scales of order the grid scale, so this component damps out quickly in time. The time-history of the RMS error of the solution is shown in Fig. (4). A remnant of the difficulty LDG has with f_{xxx} can be seen in the time history, as the error rapidly grows from 0 to a finite value at very early times, but then saturates as the component of the solution with the large error decays away. (Table 1 of Ref. [7] gives the error in the LDG solution to a diffusion equations at $t = 2$, so the rapidly changing transient error at early times is not noticeable then.) These errors may be more noticeable in problems where one is plotting not just f but gradients of f (such as in Navier-Stokes simulations where one plots the vorticity $\nabla \times \mathbf{v}$). Overall, one sees that among the schemes tested, the RDG scheme has the smallest error. In addition, it converges faster as the grid is refined. For problems involving a hyperdiffusion operator f_{xxxx} , if it is evaluated as two successive applications of an LDG or RDG implementation of a second derivative operator, the net result will be a stencil that couples 5 adjacent cells. For RDG with piecewise linear basis functions, it is possible to directly implement a hyperdiffusion operator with a stencil that involves only 3 adjacent cells. (An LDG algorithm that split the hyperdiffusion operator into 4 coupled first-order equations might be able to get a similar result with an appropriate choice of the order of upwinding in various steps.)

While the full RDG method is higher order accurate, it should be mentioned that certain properties of a diffusion equation, such as reducing extrema and thus preserving positivity, are not guaranteed by higher order methods unless limiters of some sort are applied. (Reducing extrema is related to not decreasing the entropy $S(t) = -\int dx f \log(f)$.) For some applications, simpler second-order accurate diffusion methods (which can preserve these properties without additional limiters) may be sufficient.

Acknowledgements

We thank J. C. Hosea, M. C. Zarnstorff, and S. C. Prager for supporting the initiation of this project, and we thank B. Cockburn and C.-W. Shu for helpful discussions. This work was funded by the U. S. Department of Energy Contract DE-AC02-09CH11466, through the Max-Planck/Princeton Center for Plasma Physics and the Princeton Plasma Physics Laboratory.

References

References

- [1] B. Cockburn, C.-W. Shu, The Runge–Kutta Discontinuous Galerkin Method for Conservation Laws V, *Journal of Computational Physics* 141 (1998) 199–224.
- [2] B. Cockburn, C.-W. Shu, Foreword for the special issue on discontinuous Galerkin method, *J. of Scientific Computing* 22-23 (2005) 1–3.
- [3] C. Dawson, Foreword for the special issue on discontinuous Galerkin method, *Computer Methods in Applied Mechanics and Engineering* 195 (2006) 3183.
- [4] G. W. Hammett, W. Dorland, F. W. Perkins, Fluid models of phase mixing, Landau damping, and nonlinear gyrokinetic dynamics, *Physics of Fluids B* 4 (1992) 2052.
- [5] G. W. Hammett, M. A. Beer, W. Dorland, S. C. Cowley, S. A. Smith, Developments in the gyrofluid approach to tokamak turbulence simulations, *Plasma Physics and Controlled Fusion* 35 (8) (1993) 973, <http://stacks.iop.org/0741-3335/35/i=8/a=006>.
- [6] Y. Cheng, I. M. Gamba, P. J. Morrison, Study of conservation and recurrence of Runge–Kutta discontinuous Galerkin schemes for Vlasov–Poisson systems, *Journal of Scientific Computing* 56 (2) (2013) 319–349.
- [7] B. Cockburn, C.-W. Shu, The local discontinuous Galerkin method for time-dependent convection-diffusion systems, *SIAM Journal on Numerical Analysis* (1998) 2440–2463.
- [8] H. Liu, J. Yan, The Direct Discontinuous Galerkin (DDG) Method for Diffusion with Interface Corrections, *Communications in Computational Physics*.
- [9] D. N. Arnold, F. Brezzi, B. Cockburn, L. D. Marini, Unified analysis of discontinuous Galerkin methods for elliptic problems, *SIAM Journal on Numerical Analysis* (2002) 1749–1779.
- [10] H. T. Huynh, A Reconstruction Approach to High-Order Schemes Including Discontinuous Galerkin for Diffusion, *AIAA* (2009) 1–34.
- [11] B. van Leer, S. Nomura, Discontinuous Galerkin for Diffusion, in: 17th AIAA Computational Fluid Dynamics Conference, American Institute of Aeronautics and Astronautics, Toronto, Ontario, 2005, pp. 1–30, <http://dx.doi.org/10.2514/6.2005-5108>.
- [12] M. Dumbser, D. S. Balsara, E. F. Toro, C.-D. Munz, A unified framework for the construction of one-step finite volume and discontinuous Galerkin schemes on unstructured meshes, *Journal of Computational Physics* 227 (2008) 8209–8253, <http://dx.doi.org/10.1016/j.jcp.2008.05.025>.
- [13] H.-O. Kreiss, T. A. Manteuffel, B. Swartz, B. Wendroff, J. A. B. White, Supra-Convergent Schemes on Irregular Grids, *Mathematics of Computation* 176 (1986) 537–554.
- [14] M. Zhang, C.-W. Shu, An Analysis of Three Different Formulations of the Discontinuous Galerkin method for diffusion equations, *Mathematical Models and Methods in Applied Sciences* 13 (2003) 395–413.